ARTICLES
https://doi.org/10.1038/s41589-021-00917-0
nature chemical biology

Temperature-responsive optogenetic probes of cell signaling

William Benman[1], Erin E. Berlew[1], Hao Deng[2], Caitlyn Parker[3], Ivan A. Kuznetsov[1], Bomyi Lim[2,4], Arndt F. Siekmann[3,4], Brian Y. Chow[1] and Lukasz J. Bugaj[1,4,5]✉

We describe single-component optogenetic probes whose activation dynamics depend on both light and temperature. We used the BcLOV4 photoreceptor to stimulate Ras and phosphatidyl inositol-3-kinase signaling in mammalian cells, allowing activation over a large dynamic range with low basal levels. Surprisingly, we found that BcLOV4 membrane translocation dynamics could be tuned by both light and temperature such that membrane localization spontaneously decayed at elevated temperatures despite constant illumination. Quantitative modeling predicted BcLOV4 activation dynamics across a range of light and temperature inputs and thus provides an experimental roadmap for BcLOV4-based probes. BcLOV4 drove strong and stable signal activation in both zebrafish and fly cells, and thermal inactivation provided a means to multiplex distinct blue-light sensitive tools in individual mammalian cells. BcLOV4 is thus a versatile photosensor with unique light and temperature sensitivity that enables straightforward generation of broadly applicable optogenetic tools.

Optogenetic probes permit light-induced control of intracellular biochemistry. Such probes are typically engineered from proteins that evolved to respond to their host's environmental conditions, that is to its light status[1,2], but in some cases also to temperature[3–5]. Light-responsive actuators now exist for control of protein dimerization[6–10], allostery[11,12], oligomerization[13], ion transport[14] and membrane recruitment[15,16], providing an extensive toolset for precise manipulation of an array of biological processes, including cell signaling.

Ras and phosphatidyl inositol-3-kinase (PI3K) are signaling regulators that together control essential cell processes including transcription, translation, growth, survival, proliferation and migration[17–20]. Optogenetic control of these two pathways has enabled recent discoveries of how their spatiotemporal dynamics regulate cell and tissue growth, form and disease[21–24]. Currently, optogenetic activation of Ras or PI3K is achieved through membrane recruitment of signaling effectors via light-induced protein heterodimerization[25,26]. However, this approach is limited by the necessity for two distinct proteins, which can require stoichiometric tuning of both components to permit signaling through a large dynamic range with minimal elevated basal signaling[27]. Although stoichiometric tuning is feasible in single cells, it is more challenging in tissues and organisms.

Single-component membrane translocation was recently described using the BcLOV4 photoreceptor, which translocates from the cytoplasm to membrane phospholipids under blue light in mammalian cells[15] (Fig. 1a). BcLOV4 has already served as a modular technology for light-induced activation of the Rho GTPases Rac1 (ref. [28]), RhoA[29] and Cdc42 (ref. [30]), suggesting that BcLOV4 may be adapted to regulate many additional pathways.

In this work, our initial goal was to generate and characterize BcLOV4-based probes for Ras or PI3K activation. Surprisingly, we discovered that BcLOV4 translocation and signal activation respond not only to blue light, but also to temperature, such that under sustained, long-term stimulation, BcLOV4 becomes inactivated and dissociates from the membrane as a function of increased temperature and light intensity. Through systematic characterization, we developed and validated a quantitative model that predicted BcLOV4 and downstream signaling dynamics as a function of light and temperature, providing a roadmap for BcLOV4 usage over a range of experimental conditions, particularly during long time-course experiments. We demonstrate the broad applicability and stable activation of our probes in zebrafish embryos and *Drosophila* Schneider 2 (S2) cells, which operate at low temperatures (22–30 °C). Finally, we demonstrate that temperature inactivation of BcLOV4 can be leveraged to allow multiplexing of blue-sensitive optogenetic probes in individual mammalian cells.

Results

Engineering control of Ras and PI3K signaling with BcLOV4. To generate an actuator of Ras/Erk signaling, we fused BcLOV4 to the catalytic domain of the Ras guanine nucleotide exchange factor Son of Sevenless 2 (SOS_{cat}), which activates Ras upon recruitment to the membrane (Fig. 1b)[26]. We generated an analogous probe to control PI3K signaling by replacing the SOS_{cat} domain with the inter-SH2 domain of the p85 subunit (iSH) (Fig. 1c)[25,31]. We refer to these probes as BcLOV–SOS_{cat} and BcLOV–iSH, respectively.

To test probe activity, we illuminated NIH 3T3 cells that stably expressed either BcLOV–SOS_{cat} or BcLOV–iSH, and we quantified levels of phospho-Erk (ppErk) or phosho-Akt (pAkt) using immunofluorescence imaging (Supplementary Fig. 1). In the absence of blue light, BcLOV–SOS_{cat} cells exhibited low basal levels of ppErk, similar to wild-type (WT) cells. Upon illumination, ppErk levels rose dramatically and reached their peak within 5 min (Supplementary Fig. 2), reaching levels comparable with WT cells stimulated with 10% serum (Fig. 1d). BcLOV–iSH-expressing cells also induced strong levels of pAkt, although basal activation in the absence of light was somewhat higher relative to WT cells (Fig. 1e).

[1]Department of Bioengineering, University of Pennsylvania, Philadelphia, PA, USA. [2]Department of Chemical and Biomolecular Engineering, University of Pennsylvania, Philadelphia, PA, USA. [3]Department of Cell and Developmental Biology and Cardiovascular Institute, Perelman School of Medicine at the University of Pennsylvania, Philadelphia, PA, USA. [4]Institute of Regenerative Medicine, University of Pennsylvania, Philadelphia, PA, USA. [5]Abramson Cancer Center, University of Pennsylvania, Philadelphia, PA, USA. ✉e-mail: bugaj@seas.upenn.edu

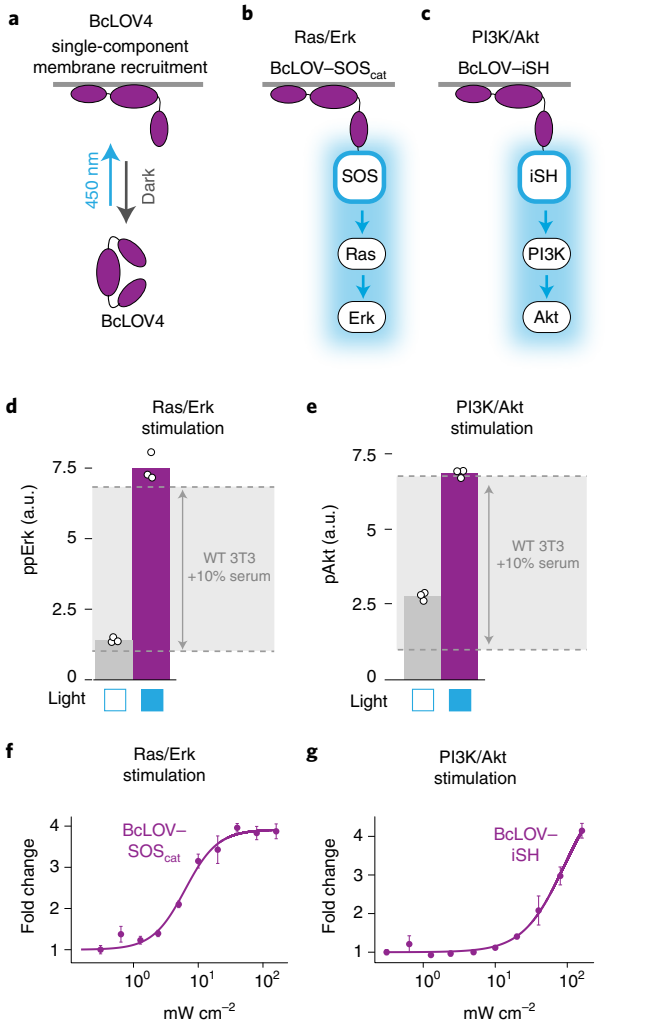

Fig. 1 | Single-component BcLOV4 fusions allow control of Ras and PI3K signaling. a, BcLOV4 binds the cell membrane when exposed to blue light. The three BcLOV4 domains represent the LOV, DUF and RGS domains, as previously described[15]. **b**, Light-induced membrane recruitment of BcLOV4 fused to the SOS_{cat} catalytic domain will induce Ras/Erk signaling. **c**, Analogous recruitment of the iSH domain will induce PI3K/Akt signaling. **d**,**e**, Five minutes of blue-light stimulation (160 mW cm^{-2} at 20% duty cycle) increases intracellular ppErk levels in cells that express BcLOV-SOS_{cat} (**d**) and increases pAkt in cells that express BcLOV-iSH (**e**). a.u., arbitrary units. Gray zone indicates the change in ppErk or pAkt in wild-type cells that were stimulated with 10% calf serum for 10 min. Data represent means of three biologically independent replicates, each representing the mean signal intensity from approximately 2,000 to 4,000 single cells. **f**,**g**, Light intensity dose-response of (**f**) ppErk fold-change induction in BcLOV-SOS_{cat}-expressing cells or (**g**) pAkt fold-change induction in BcLOV-iSH cells at 100% duty cycle after 5 min of illumination. Data represent means ± s.d. of three biologically independent replicates, each representing the mean signal intensity from approximately 300 to 500 single cells. All stimulation in **a**–**g** was achieved using the optoPlate-96. All stimulation and environmental conditions for all figures can be found in Supplementary Table 1.

These results suggest that our BcLOV-derived probes stimulate physiologically relevant levels of pathway activation while minimally disrupting endogenous cell physiology in the dark state.

To better characterize light-induced stimulation of BcLOV–SOS_{cat} and BcLOV–iSH, we measured the dose-response of signal activation as a function of light intensity. We found that BcLOV–SOS_{cat} achieves half-maximal pathway stimulation with 7 mW cm^{-2} of blue light and saturates near 40 mW cm^{-2} with a fourfold signal induction (Fig. 1f). Conversely, we estimate that BcLOV–iSH reaches half-maximal signal induction with 80 mW cm^{-2}, although we did not reach saturation at the highest levels of stimulation (160 mW cm^{-2}) (Fig. 1g). Taken together, given the large fold-change induction, minimal basal level of stimulation and single-component nature, BcLOV4-based probes offer several beneficial qualities for optogenetic stimulation of Ras and PI3K signaling.

Optogenetic activation decays during extended stimulation. We next asked how BcLOV4-based probes regulate signaling through time. We used recently described illumination devices for microwell plates (the optoPlate-96) to perform time-course stimulation experiments[27]. After stimulation, cells were immunostained and quantified to assess pathway activity (Fig. 2a).

We were surprised to find that, despite constant stimulation for 60 min, cells that expressed BcLOV–SOS_{cat} showed an initial increase followed by rapid and complete decay of ppErk (Fig. 2b and Supplementary Fig. 3). To determine whether transient signaling was caused by BcLOV4 or alternative mechanisms (for example, negative feedback within the Ras/Erk pathway), we compared activation dynamics with those achieved with an orthogonal optogenetic system, iLID/sspB (nano), a commonly used blue-light inducible heterodimerizing protein pair[6], which can be adapted to recruit SOS_{cat} to the membrane (iLID–SOS_{cat}[23]; Supplementary Fig. 4). By contrast to BcLOV–SOS_{cat}, iLID–SOS_{cat} produced stable signaling under identical illumination conditions (see Supplementary Table 1 for detailed experimental conditions for all experiments), indicating that Ras/Erk signal decay was a feature of BcLOV4 stimulation. Similarly, sustained illumination of BcLOV–iSH cells led to an initial increase followed by a rapid decrease in pathway activity, whereas stimulation with an analogous iLID-based probe (iLID–iSH; Supplementary Fig. 4) resulted in sustained activity (Supplementary Fig. 5A,B). These results further indicate that transient activation dynamics were a function of BcLOV4 activation and not the pathway under study.

To understand the nature of signal decay, we performed a series of experiments using the BcLOV–SOS_{cat} probe. We first asked whether BcLOV–SOS_{cat} inactivation could be reversed after removal of the light stimulus. We stimulated cells with blue light until the signal decayed, withdrew light for either 0.5, 1 or 3 h and then restimulated for 10 min (Fig. 2c). As before, the initial 45 min of blue light led to a pulse of ppErk signal. However, only ~10% of the original signal could be obtained upon restimulation even after 3 h of light withdrawal. This small amount of reactivation was partially a result of new protein production rather than reversal of inactivated BcLOV–SOS_{cat} (Supplementary Fig. 6). These results suggest that BcLOV4 can undergo a spontaneous transition into an uncharacterized, long-lived inactivated state.

We next asked whether certain experimental parameters could modulate the observed signal decay rate. We noticed that pathway decay kinetics could change as a function of the illumination settings of individual experiments. Because higher light intensity can also cause heating of the sample[27], we tested the effects of both temperature and light on BcLOV–SOS_{cat} stimulation kinetics. To perform optogenetic time-course experiments at specific temperatures, we adapted the optoPlate-96 to precisely control both illumination and sample temperature (Fig. 2d,e and Supplementary Fig. 7). Briefly, we decoupled sample heating from the illumination profile by designating 24 light-emitting diode (LED) positions for light stimulation and using the remaining 72 LED positions as heating elements (Fig. 2d). Illumination of the 72 'heater' LEDs over 3,000 intensity levels correlated linearly with sample temperature in the wells above the 24 'stimulation' LEDs ($R^2 = 0.99$) (Fig. 2e).

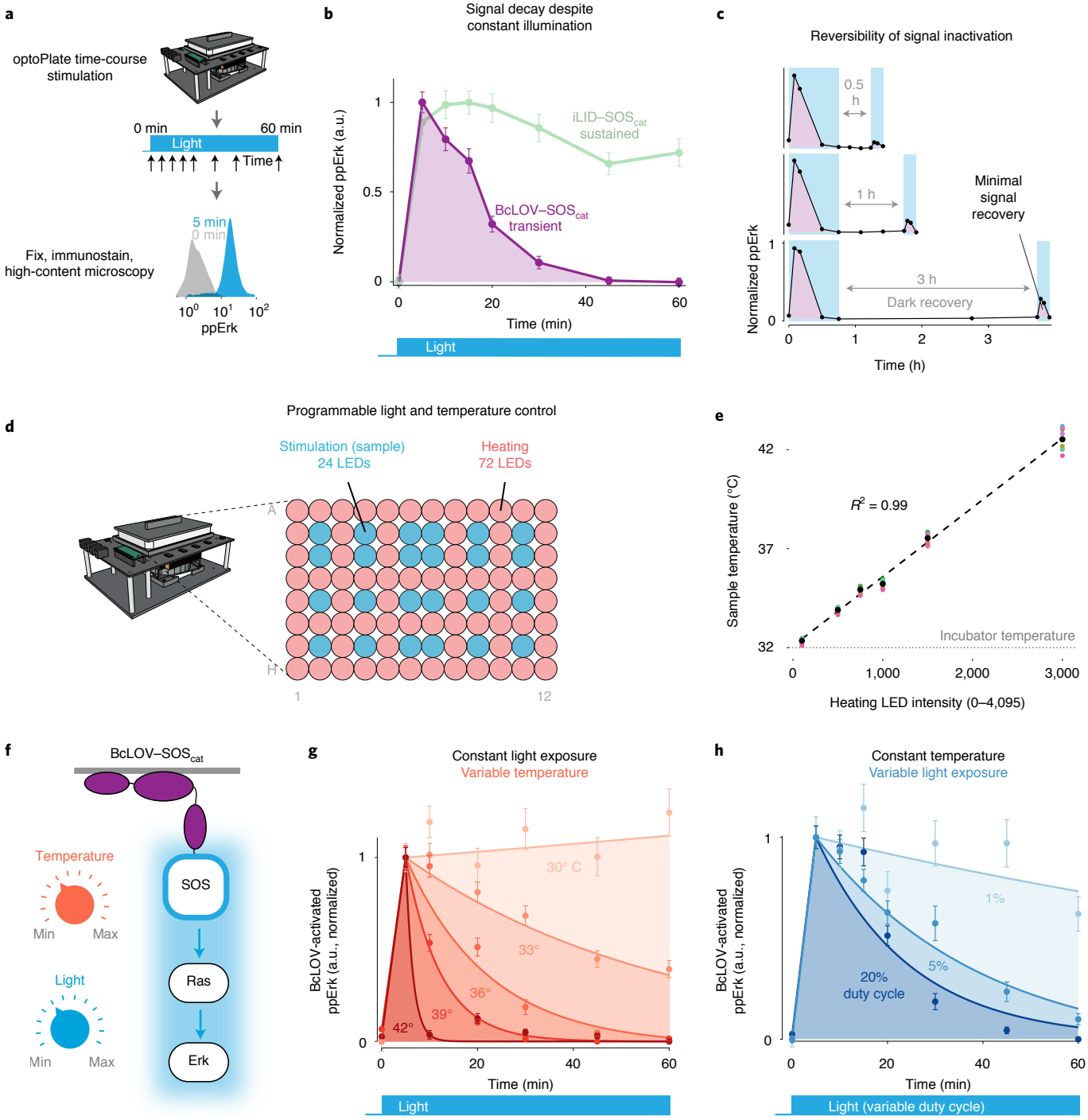

Fig. 2 | BcLOV-induced signaling dynamics depend on temperature and light exposure. a, Schematic of experimental protocol. **b**, Sustained stimulation of BcLOV–SOS$_{cat}$ (160 mW cm^{-2} at 20% duty cycle) reveals that the ppErk signal decays rapidly after an initial increase, whereas activation by iLID–SOS$_{cat}$ remains sustained. **c**, Recovery (dark) periods of up to 3 h after signal decay do not permit recovery of activatable BcLOV–SOS$_{cat}$, suggesting that BcLOV4 inactivation is effectively irreversible. **d**, BcLOV–SOS$_{cat}$ signal dynamics were examined under variable light and temperature conditions. **e**, Schematic for how the optoPlate-96 was repurposed to allow independent control of experimental light and temperature conditions. For more information, see Supplementary Fig. 7. **f**, Steady-state sample temperature was a linear function of the intensity of the 72 heater LEDs (precise intensity–temperature relationship should be determined empirically for each individual optoPlate). See Methods. **g**, At a given light exposure level (here, 160 mW cm^{-2} at 20% duty cycle), BcLOV–SOS$_{cat}$ signal decays more rapidly at higher temperatures. **h**, At a given temperature (here, 36 °C), BcLOV–SOS$_{cat}$ decay increases with increased light exposure (variable duty cycles of 160 mW cm^{-2} light). Data points in (**b**), (**c**), (**g**) and (**h**) represent the mean ± s.e.m. of ~1,000–4,000 individual cells. Traces in (**g**) and (**h**) are exponential decay functions fit to data points at each temperature and duty cycle, as described in the Methods section. Data are normalized between the minimum and maximum of each trace. Normalization was performed separately for each temperature and duty cycle to highlight the change in the rate of BcLOV–SOS$_{cat}$ inactivation rather than absolute signal. Absolute signal traces can be found in Supplementary Fig. 8. a.u., arbitrary units.

Strikingly, we observed that BcLOV–SOS$_{cat}$ decay kinetics were strongly correlated to sample temperature, where signal decay was faster at higher temperatures (Fig. 2f,g and Supplementary Fig. 8A). At the extremes, ppErk decayed with a half-life of ~6 min at 42 °C, whereas decay was minimal at 30 °C. We observed strong ppErk signal induction at all temperatures tested, suggesting that temperature only impacted BcLOV4 function in its lit, activated form (Supplementary Fig. 8A). The BcLOV–iSH probe was also temperature-sensitive (Supplementary Fig. 8B). By contrast, iLID–SOS- and iLID–iSH-induced signaling was sustained at both high and low temperatures (Supplementary Fig. 8C,D), further indicating that temperature sensitivity is a property of BcLOV4 control. Finally, we used a live-cell reporter of Erk activity (ErkKTR[32]) as an orthogonal readout to verify that, in contrast to temperature-regulated inactivation, optogenetic inactivation (removal of blue light) was reversible over multiple illumination cycles at both high (37 °C) and low (30 °C) temperatures (Supplementary Fig. 9).

We also observed that the BcLOV–SOS$_{cat}$ signal decay rate was dependent on light intensity, where higher intensity led to rapid decay, whereas lower intensity led to more sustained stimulation (Fig. 2h and Supplementary Fig. 8E). The low light achieved sustained signaling at the expense of signal amplitude (Supplementary Fig. 8E), although we note that this tradeoff will be specific to the pathway under study. For example, in a previous report, comparable sparse illumination conditions (1.6% duty cycle) yielded saturating activation levels of BcLOV-regulated Rho GTPase signaling[28,29].

Because signal decay was observed with both the BcLOV–SOS$_{cat}$ and BcLOV–iSH probes, but not with analogous iLID-based probes (Fig. 2b and Supplementary Fig. 8C), we suspected that the observed light- and temperature-dependent decay kinetics were a property of the BcLOV4 photosensor itself. We thus quantified membrane translocation of BcLOV–mCherry under various light and temperature conditions (Fig. 3a and Supplementary Fig. 10). In accordance with our signaling results, sustained illumination resulted in sustained membrane localization at low temperatures (25 °C) but only transient localization at 37 °C, with inactivated BcLOV4 returning to the cytoplasm after ~30 min (Fig. 3b,c, Supplementary Fig. 10 and Supplementary Movie 1). Similarly, when we varied light intensity at a constant temperature, increased intensity (duty cycle) increased the decay rate of membrane translocation (Fig. 3d). Decay of membrane fluorescence was not due to BcLOV4 degradation (Supplementary Fig. 11). As before, we observed initial membrane recruitment at all temperatures (Supplementary Fig. 10), and BcLOV4 inactivation was irreversible for at least 3 h (Supplementary Fig. 12). Together, these data demonstrate that BcLOV4 is not only a photosensor, but also a temperature sensor.

Modeling dependence of BcLOV on temperature and light. To explain and predict BcLOV–mCherry translocation dynamics, we developed a computational model. We reasoned that, in addition to the dark and lit states, a third state of BcLOV4 could account for our observations of light- and temperature-dependent decay kinetics (Fig. 3e). This third state, which we call the temperature-inactivated (TI) state, is only accessible from the lit (membrane-bound) state, and transition to the TI state is irreversible at the timescales we consider (Fig. 2c, Supplementary Figs. 6 and 12). We predicted that the rate of entry into the TI state (k_3) would increase as a function of temperature. Thus, because more light increases the amount of BcLOV4 in the lit state, and higher temperature increases the transition rate from the lit to the TI state, our model could explain why both increased light and temperature can increase the decay rate of BcLOV4 membrane translocation. For details on model development, see Fig. 3e–g, Supplementary Fig. 10 and Methods.

We parameterized our model by fitting values for k_1, k_2 and k_3 to live-cell data of BcLOV–mCherry translocation dynamics over a range of temperatures (25–40 °C) and light exposures (1.1%, 3.3%, 10% duty cycle) (Fig. 3e,f, Supplementary Figs. 10 and 13). Across experimental conditions, we obtained consistent values for k_1 and k_2 (Methods), which correspond closely to reported values of BcLOV4 membrane translocation and dissociation (half-times of ~1 s for association and ~1 min for dissociation)[15]. As expected, k_3 showed a strong exponential dependence on temperature (Supplementary Fig. 13). We then used our parameterized model to generate a two-dimensional heatmap of predicted BcLOV4 decay rate as a function of temperature and light dose during sustained stimulation (Fig. 3g). This heatmap represents a roadmap of translocation dynamics that can be used to predict the behavior of BcLOV4-based probes.

To validate our model and predict signaling dynamics downstream of BcLOV–SOS$_{cat}$ stimulation, we integrated our model of membrane translocation with a model of Ras/Erk signal transmission (Fig. 4a). We modeled the Ras/Erk pathway with a transfer function that represents signal transmission from membrane-localized SOS$_{cat}$ to Erk phosphorylation as a dynamic filter. Previous work defined the Ras/Erk module as a second-order low-pass filter (LPF) with a 2-mHz cutoff frequency[26]. However, this previous work applied SOS$_{cat}$ membrane localization as an input and measured nuclear localization of fluorescently tagged Erk2 as the output, whereas in our case the output was cytoplasmic levels of endogenous ppErk. Thus, to choose the most appropriate model, we performed dynamic stimulation of BcLOV–SOS$_{cat}$ and fitted either first- or second-order LPF models to the data. We found that signal transmission was best modeled by a first-order LPF with a cutoff frequency of 2 mHz (Fig. 4b,c). Because first-order filters transmit fast signal dynamics more efficiently than analogous second-order filters (Fig. 4b), our results suggest that the Ras/Erk pathway can transmit fast signal fluctuations (less than ~4 min) more effectively than previously measured[26]. Our results may differ from previous measurements because of additional biochemical steps required to transduce phosphorylation into nuclear translocation of fluorescently tagged Erk, compared with the direct observation of Erk phosphorylation in our work. Notably, our model captured both the fast timescale dynamics of ppErk fluctuations, as well as the slow timescale decay of ppErk due to progressive BcLOV4 inactivation (Fig. 4c).

Our integrated model of membrane translocation and Erk activation predicted how specific light and temperature inputs shape BcLOV–SOS$_{cat}$-induced ppErk dynamics. We used this model to generate a heatmap of ppErk decay rate as a function of temperature and light dose during constant illumination (Fig. 4d). To validate our model, we performed stimulation time-course experiments at temperature and light conditions that were sampled from regions of our heatmap with diverse decay rates. Measured ppErk decay rates matched closely with the rates predicted by our model over all experimental conditions tested (Fig. 4d and Supplementary Fig. 14). Phototoxicity was not observed under the illumination conditions used in this study (Supplementary Fig. 15). Together, our data and models comprehensively describe how BcLOV4 and optogenetic probes thereof will behave as a function of light and temperature condition. We note, however, that decay rates will probably vary between pathways due to pathway-specific biochemistry and must thus be determined empirically.

BcLOV4-based signal activation in model organisms. The single-component nature and low rate of spontaneous decay at <30 °C position BcLOV4-based tools as highly suited for experiments in tissues and model organisms that operate at lower temperatures. We thus tested the performance of BcLOV4 and BcLOV–SOS$_{cat}$ in both zebrafish embryos and *Drosophila* S2 cells. BcLOV–mCherry expressed well in zebrafish embryos and, upon illumination, rapidly translocated to the membrane in all cells (Fig. 5a and Supplementary Movie 2). Membrane translocation was

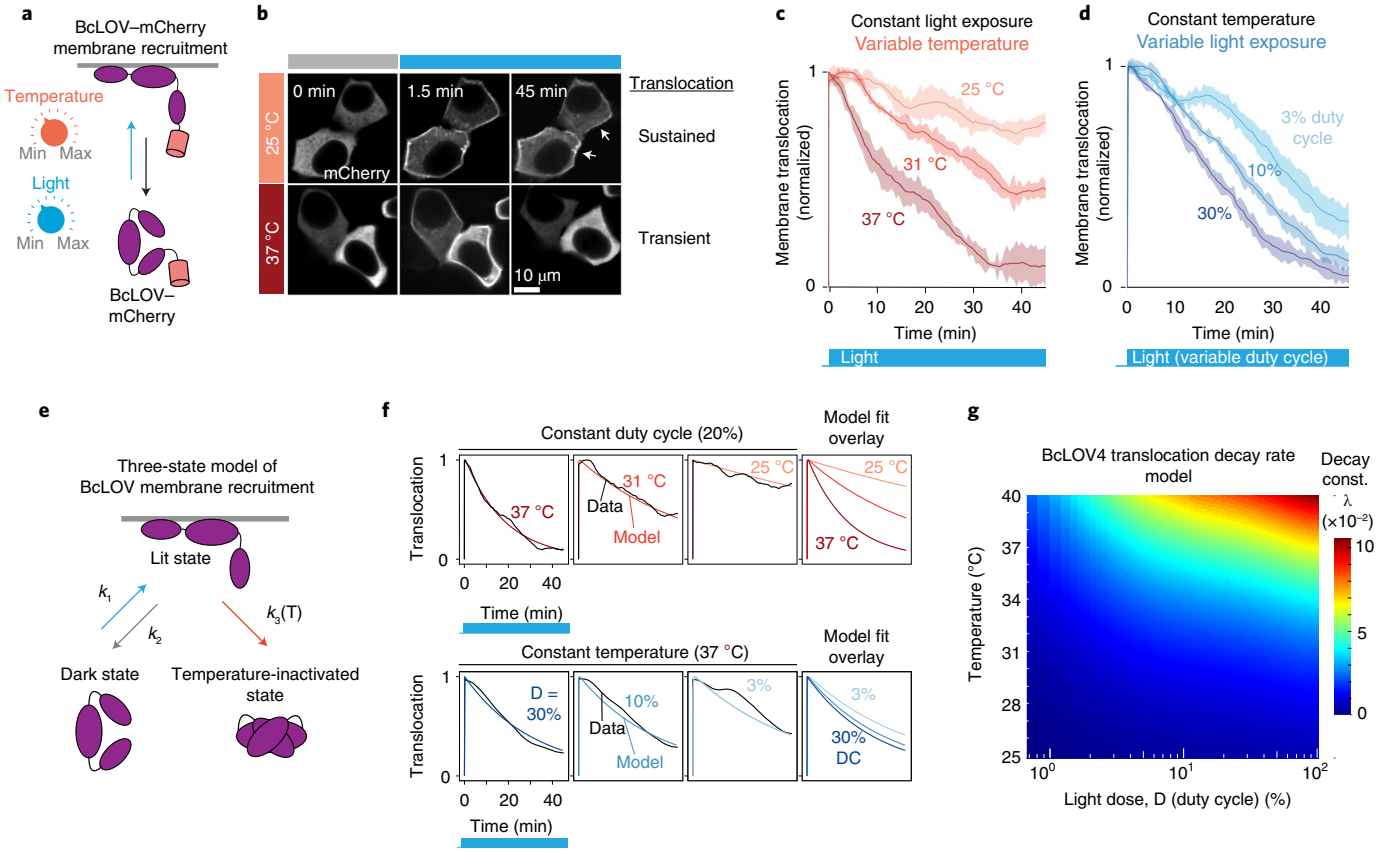

Fig. 3 | BcLOV4 membrane translocation dynamics depend on temperature and light exposure. a, BcLOV–mCherry membrane recruitment was quantified at various temperatures and light exposures using live-cell imaging. **b**, Representative images of membrane recruitment at low and high temperatures. Activation at 25 °C permitted sustained membrane recruitment, whereas recruitment at 37 °C was transient (stimulation performed at 1.45 W cm^{-2} and 3% duty cycle). Image brightness was adjusted at each time point for clarity to account for photobleaching. **c**, Quantification of membrane recruitment at various temperatures (1.45 W cm^{-2} at 3% duty cycle) reveals a temperature-dependent decay of membrane translocation. **d**, Quantification of membrane recruitment at various light exposures (at 36 °C and 1.45 W cm^{-2}) shows light-dependent decay of BcLOV–mCherry translocation. Each trace is the mean membrane fluorescence ± s.e.m. of three biologically independent samples, with each replicate representing the mean of ~100 cells. See Supplementary Fig. 10 for unnormalized traces and quantification workflow. **e**, Schematic of a three-state model of BcLOV4 membrane translocation. **f**, Fitting the model to live-cell translocation data provides parameter values for k_1, k_2 and k_3 (T). **g**, Heatmap depicts the decay rate of BcLOV4 membrane localization as a function of temperature and light exposure. Decay rates were calculated by simulating sustained illumination over a range of duty cycles and temperatures and fitting the modeled decay rate to a single exponential decay. Color indicates the decay constant **λ** (1 divided by the time to reach 37% of maximum signal). Larger **λ** indicates faster decay. See Supplementary Figs. 10, 13 and Methods for imaging and model details.

sustained through 90 min of illumination, as expected from our experiments in mammalian cells (Fig. 5b). To determine whether BcLOV–SOS$_{cat}$ could stimulate Ras signaling in zebrafish, we coexpressed BcLOV–SOS$_{cat}$ with the ErkKTR reporter, which has previously been used in zebrafish (Fig. 5c)[33]. In cells that coexpressed BcLOV–SOS$_{cat}$ and ErkKTR, we observed rapid and reversible ErkKTR translocation that could be stimulated over multiple cycles (Fig. 5d and Supplementary Movie 3), consistent with our data from mammalian cells. Notably, over 90 min of sustained stimulation, Erk activity remained high, demonstrating that both BcLOV–SOS$_{cat}$ translocation and signal activation could be maintained (Fig. 5). We also expressed BcLOV4 probes in *Drosophila* S2 cells as an orthogonal model system that grows at temperatures permissive to stable BcLOV4 translocation, and we again observed sustained BcLOV–mCherry membrane localization through 90 min of blue-light illumination (Fig. 5f,g). Furthermore, expression and sustained stimulation of BcLOV–SOS$_{cat}$ allowed sustained activation of ppErk (Fig. 5h). Together, these data show that BcLOV4-based probes can serve as simple and sensitive optogenetic probes across diverse cells, tissues and organisms of study.

Optogenetic multiplexing using BcLOV4. Finally, we reasoned that the unique light- and temperature-responsiveness of BcLOV4 could be leveraged as a control mode to regulate multiple optogenetic proteins in single cells. Currently, such multiplexing can be achieved using optogenetic probes with different activation spectra (for example, blue- and red-absorbing). However, there is a relative lack of optogenetic proteins that respond to red-shifted (nonblue) light, and the absorption spectra of these few probes can also reach into the 400–500 nm (blue) range, thus challenging orthogonal multiplexing with blue-sensitive probes[27,34]. An arguably simpler approach would be to multiplex control of distinct blue-sensitive probes. To demonstrate how temperature regulation of BcLOV4 enables such multiplexing, we coexpressed BcLOV4 with one of two blue-light sensitive tools: an iLID/sspB membrane binding system (Supplementary Fig. 4) or cryptochrome 2 (Cry2), which forms large aggregates when activated by blue light[13]. Coexpression of BcLOV4–mCherry and green fluorescent protein (GFP)-tagged iLID/sspB (iLID/sspB–GFP) allowed control of three activation states: none (dark), both (blue light) or iLID-ONLY, achieved by sequential heat inactivation of BcLOV4 and subsequent light stimulation of iLID (Fig. 6a–c).

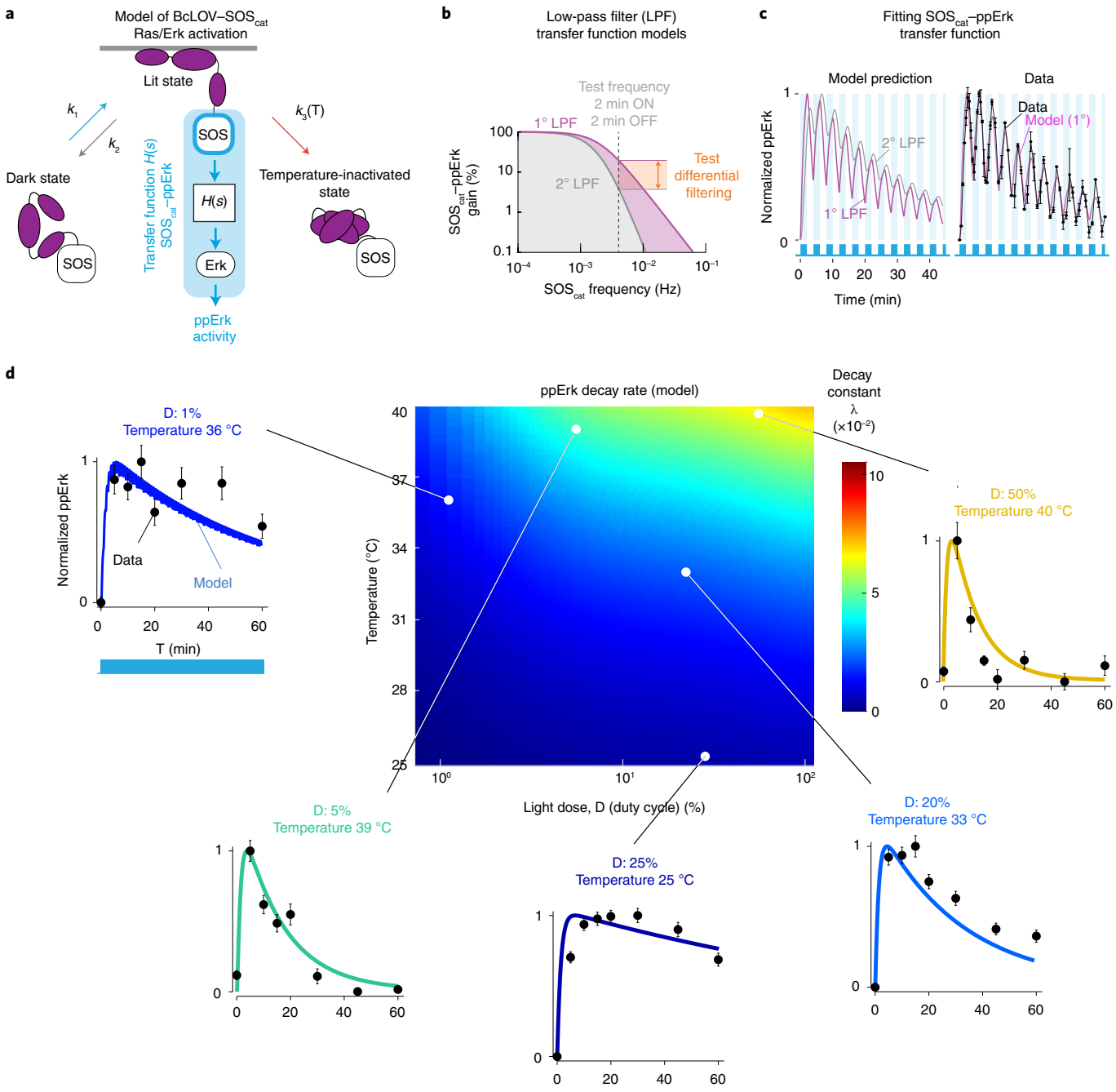

Fig. 4 | Modeling predicts BcLOV-SOS$_{cat}$-induced ppErk dynamics and reveals dynamic filtering properties of Ras/Erk signaling. a, A model of ppErk activation was developed by integrating the BcLOV4 membrane translocation model with a transfer function model that describes the input/output response of SOS$_{cat}$ membrane localization (input) to ppErk activation (output). **b**, Filtering properties of a 1° versus 2° LPF. 1° LPFs attenuate high-frequency inputs less than 2° LPFs. **c**, A 1° LPF with 2-mHz cutoff frequency best describes ppErk dynamics when stimulated with fast 2 min ON/2 min OFF BcLOV-SOS$_{cat}$ oscillations. Data points are the mean ± s.d. of three biologically independent replicates, with each replicate representing the mean of ~1,000–2,000 cells. **d**, Heatmap depicts the predicted Erk activation dynamics resulting from BcLOV4 membrane translocation dynamics over the indicated light and temperature conditions. Plots show model predictions of Erk activation at the indicated experimental conditions, and data points show experimental results. Data points represent means ± s.e.m. of ~1,000–4,000 cells. Unnormalized plots are presented in Supplementary Fig. 14. See Methods for model details.

Coexpression of BcLOV–GFP with Cry2–mCherry allowed control of all four possible activation states (Fig. 6d,e). In this arrangement, the BcLOV-ONLY state can be achieved because of differential ON-kinetics of fast BcLOV4 translocation versus the slower formation of large Cry2 clusters. We note that although the Cry2–mCherry displayed in Fig. 6e was imaged at 45 min, the time at which clusters appear is highly variable (approximately minutes to tens of minutes) and depends on Cry2 concentration. Nevertheless, because Cry2 clustering kinetics are slower than BcLOV translocation (approximately seconds), they permit a BcLOV-ONLY state at relatively short timescales.

Discussion

We describe the application of BcLOV4 membrane translocation to generate single-component probes for optical control over Ras/Erk or PI3K signaling. We characterized these probes in mammalian

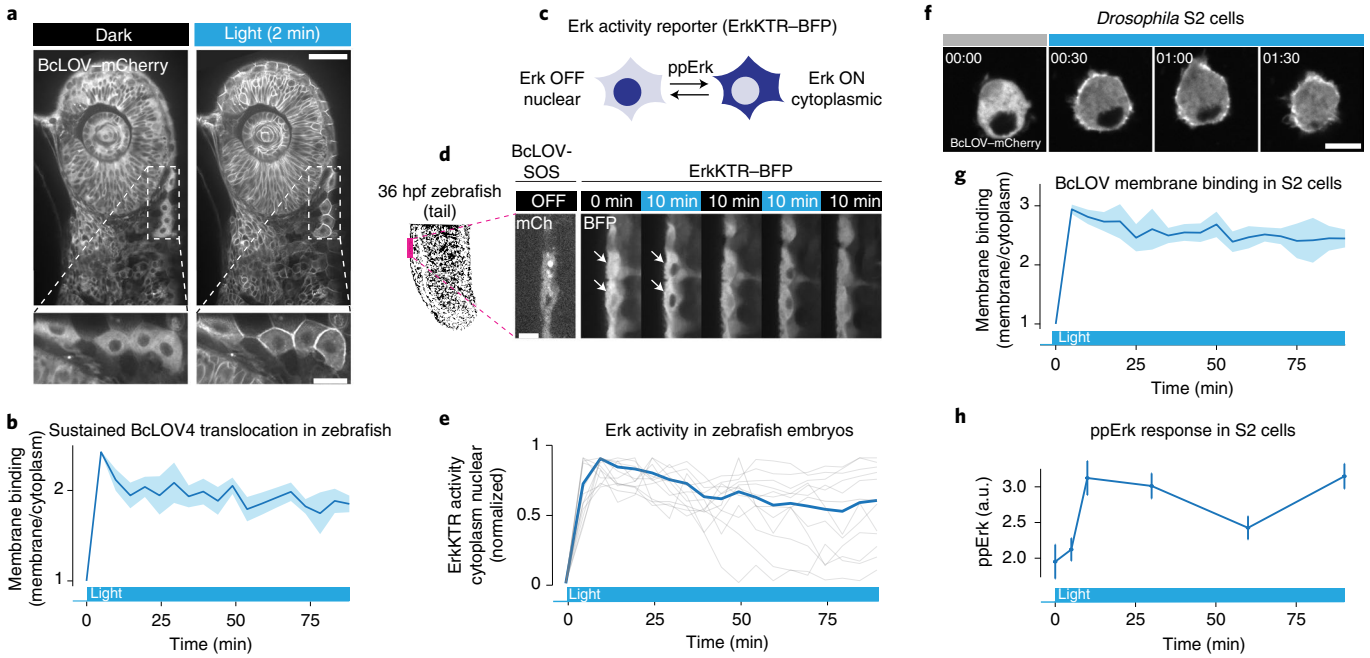

Fig. 5 | BcLOV4 and BcLOV–SOS$_{cat}$ in zebrafish embryos and *Drosophila* cells. a, Blue-light-induced membrane translocation of BcLOV–mCherry in a zebrafish embryo (24 h post fertilization (hpf)). Scale bar, 50 µm; inset scale bar, 20 µm. **b**, BcLOV–mCherry translocation is sustained over 90 min in zebrafish embryos. Data represent mean ± s.d. of ten cells. **c**, Schematic of ErkKTR activity. ErkKTR is nuclear when Erk signaling is off and translocates to the cytoplasm when Erk is activated. **d**, The Ras/Erk pathway can be reversibly stimulated over multiple cycles in zebrafish embryos (24 hpf) that coexpress BcLOV–SOS$_{cat}$ and ErkKTR–BFP, as measured by ErkKTR–BFP translocation. White arrows highlight nuclei where ErkKTR translocation is evident. Scale bar, 10 µm. **e**, Sustained illumination of BcLOV–SOS$_{cat}$ permits sustained elevated Erk activity in 24 hpf zebrafish embryos. Plot shows ErkKTR cytoplasmic/nuclear ratios of 12 single cells (light gray; blue trace represents mean) measured over two experiments. Trajectories are normalized between 0 and 1 to permit comparison between experiments. For (**a**)–(**e**) stimulation was performed using 1.45 W cm^{-2} 488 nm light at 1.5% duty cycle. **f**, BcLOV–mCherry membrane translocation in *Drosophila* S2 cells stimulated with blue light (1.45 W cm^{-2} at 3% duty cycle) for 90 min. Scale bar, 10 µm. **g**, Quantification of (**f**) shows sustained membrane translocation in S2 cells. Data represent mean ± s.d. of ten cells. **h**, Sustained stimulation of BcLOV–SOS$_{cat}$ in S2 cells shows sustained elevated ppErk levels over 90 min, measured by immunofluorescence. Data represent the mean ± s.d. of three biologically independent samples, with each replicate representing the mean of ~100–200 cells.. Stimulation was performed at (160 mW cm^{-2} at 20% duty cycle). All experiments shown in Fig. 5 were performed at room temperature. a.u., arbitrary units.

cells and found that the BcLOV4-based probes can provide signaling through a large, physiologically relevant dynamic range with low basal signaling and high photosensitivity. In addition, BcLOV4-based probes are single-protein systems, eliminating the need for stoichiometric tuning of analogous multicomponent tools. Such tuning can be difficult in model organisms like *Drosophila* and zebrafish, in which we show that BcLOV4-based probes function well. More generally, our work adds to the growing library of BcLOV4-based optogenetic signaling tools[28–30], highlighting BcLOV4 as a modular optogenetic actuator of effector/membrane interaction to regulate signaling across biological models, including yeast, flies, zebrafish and mammalian cells[15,28].

We discovered that BcLOV4 is a temperature sensor in addition to its known role as a photosensor. Although temperature-dependence has been observed in certain photosensors and optogenetic probes, this dependence mostly manifests as decreased protein stability or photoreactivity at elevated temperatures[3,10,35–39]. By contrast, BcLOV4 folds and translocates rapidly when exposed to light at all temperatures, but then, under sustained illumination, enters a long-lived inactive state and reverts to the cytoplasm at a rate that increases with both temperature and light dose (Figs. 2, 3 and Supplementary Fig. 10). This behavior is consistent with a temperature-dependent photoinactivation in which, once BcLOV4 is at the membrane in its active state, elevated temperatures accelerate its transition into a state that is incompatible with membrane binding. Although the structural details of such inactivation remain unknown, light-induced oxidation[40] and thermal denaturation during the photocycle[41] have both been observed in blue-light photosensors and could conceivably play a role in BcLOV4 temperature inactivation.

We developed quantitative models of BcLOV4 membrane translocation and signal activation to predict activity as a function of light and temperature. We found that sustained, whole-cell illumination will result in sustained translocation only under low light exposure or low temperature. These conditions may explain why BcLOV4 inactivation was not previously noticed, as its use to date has been performed at either ≤30 °C or over short periods, necessitated only sparse illumination (~1% duty cycle), or used subcellular regions of stimulation, which preserves unstimulated, activatable BcLOV4 outside the region of illumination[15,28,29].

In addition to shaping long-term activation dynamics, BcLOV4 temperature sensitivity can be leveraged to allow multiplexing of blue-light sensitive tools in single cells, allowing control of three or four distinct cell states using a single blue-light channel. Our approach is complementary to a recent report wherein distinct transcriptional targets were activated using blue light with different temporal patterns[42]. Our method provides similar capability but at the post-translational level; for example, for the study of how multiple signals (for example, Ras and PI3K) are integrated in single cells. We note that when attempting four-state control (with Cry2), the duration of the BcLOV4-ONLY state can be altered by tuning the ability of Cry2 to form large clusters, either by changing Cry2 concentration or through the use of Cry2 variants that change its propensity for cluster formation[43].

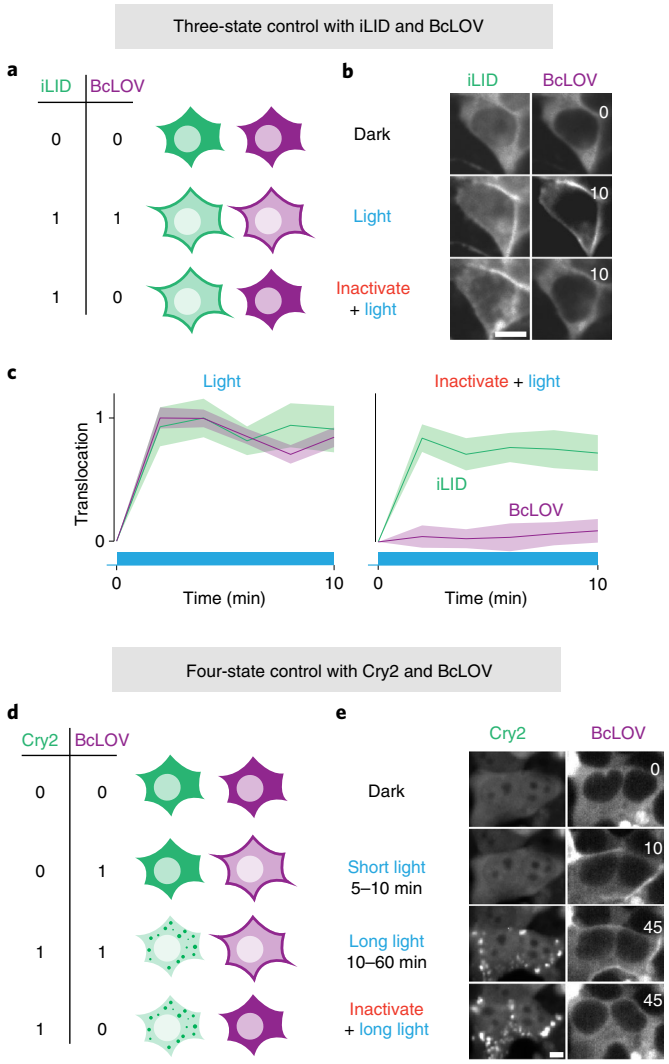

Fig. 6 | BcLOV4 temperature sensitivity enables orthogonal multiplexing of multiple blue-light sensitive tools in single cells. a, Schematic of how coexpression of BcLOV4 and iLID/sspB can allow blue-light control of three separate cell states. **b**, Coexpression in of BcLOV-mCherry and iLID/sspB-GFP in HEK 293 T cells demonstrates three-state control using blue light with or without temperature inactivation. Light stimulation was performed at 37 °C using 1 s of blue light (1.45 W cm^{-2}) every 30 s for 10 min in the presence or absence of prior BcLOV inactivation. Prior inactivation was achieved by illuminating with these same light settings for 1 h. **c**, Quantification of light-induced membrane binding (activation) of BcLOV4 and iLID in the absence (left) or presence (right) of prior heat inactivation. Traces are the normalized mean ± s.e.m. of three biologically independent replicates, with each replicate representing the mean of ~100 cells. **d**, Schematic of how coexpression of BcLOV4 and Cry2 can allow blue-light control of four separate cell states. **e**, Coexpression of BcLOV-GFP and Cry2-mCherry in HEK 293 T cells demonstrates four-state control. 'Short light' (10 min) and 'long light' (45 min) exposure were both achieved using 100 ms of light (1.45 W cm^{-2}) every 30 s at 30 °C. To achieve the Cry2-ONLY state (bottom row), images were acquired after BcLOV was inactivated using 1 s of blue light (1.45 W cm^{-2}) every 30 s for 45 min at 37 °C. Scale bar, 10 µM. See Methods and Supplementary Table 1 for full illumination conditions. Time is given in minutes. The multiplexing experiments depicted are representative of two independent experiments for each pair of optogenetic proteins.

Combined with previous work, our studies provide a roadmap for how to use BcLOV4-based optogenetic tools. BcLOV4 membrane recruitment can be faithfully and precisely controlled over short durations (less than ~30 min) across temperatures but requires low temperatures or sparse illumination for sustained (>30 min) stimulation. Specific BcLOV4 translocation dynamics over a range of light and temperature conditions can be predicted using our three-state model (Fig. 3e–g). Although our work predicts a temperature-inactivated state of BcLOV4, future studies are required to understand the molecular basis for this temperature sensitivity. Such studies will inform protein engineering efforts to modulate BcLOV4 temperature-responsiveness for enhanced optical and thermal control across biological systems.

Online content

Any methods, additional references, Nature Research reporting summaries, source data, extended data, supplementary information, acknowledgements, peer review information; details of author contributions and competing interests; and statements of data and code availability are available at https://doi.org/10.1038/s41589-021-00917-0.

Received: 7 April 2021; Accepted: 6 October 2021;
Published online: 22 December 2021

References

1. Christie, J. M., Salomon, M., Nozue, K., Wada, M. & Briggs, W. R. LOV (light, oxygen, or voltage) domains of the blue-light photoreceptor phototropin (nph1): binding sites for the chromophore flavin mononucleotide. *Proc. Natl Acad. Sci. USA* **96**, 8779–8783 (1999).
2. Schwerdtfeger, C. & Linden, H. VIVID is a flavoprotein and serves as a fungal blue light photoreceptor for photoadaptation. *EMBO J.* **22**, 4846–4855 (2003).
3. Dietler, J. et al. A light-oxygen-voltage receptor integrates light and temperature. *J. Mol. Biol.* **433**, 167107 (2021).
4. Hunt, S. M., Elvin, M., Crosthwaite, S. K. & Heintzen, C. The PAS/LOV protein VIVID controls temperature compensation of circadian clock phase and development in *Neurospora crassa*. *Genes Dev* **21**, 1964–1974 (2007).
5. Gutiérrez-Medina, B. & Candia, C. N. H. Aggregation kinetics of the protein photoreceptor Vivid. *Biochim. Biophys. Acta Proteins Proteom* **1869**, 140620 (2021).
6. Guntas, G. et al. Engineering an improved light-induced dimer (iLID) for controlling the localization and activity of signaling proteins. *Proc. Natl Acad. Sci. USA* **112**, 112–117 (2015).
7. Kennedy, M. J. et al. Rapid blue-light-mediated induction of protein interactions in living cells. *Nat. Methods* **7**, 973–975 (2010).
8. Shimizu-Sato, S., Huq, E., Tepperman, J. M. & Quail, P. H. A light-switchable gene promoter system. *Nat. Biotechnol.* **20**, 1041–1044 (2002).
9. Strickland, D. et al. TULIPs: tunable, light-controlled interacting protein tags for cell biology. *Nat. Methods* **9**, 379–384 (2012).
10. Kawano, F., Suzuki, H., Furuya, A. & Sato, M. Engineered pairs of distinct photoswitches for optogenetic control of cellular proteins. *Nat. Commun.* **6**, 6256 (2015).
11. Zhou, X. X., Chung, H. K., Lam, A. J. & Lin, M. Z. Optical control of protein activity by fluorescent protein domains. *Science* **338**, 810–814 (2012).
12. Wu, Y. I. et al. A genetically encoded photoactivatable Rac controls the motility of living cells. *Nature* **461**, 104–108 (2009).
13. Bugaj, L. J., Choksi, A. T., Mesuda, C. K., Kane, R. S. & Schaffer, D. V. Optogenetic protein clustering and signaling activation in mammalian cells. *Nat. Methods* **10**, 249–252 (2013).
14. Boyden, E. S., Zhang, F., Bamberg, E., Nagel, G. & Deisseroth, K. Millisecond-timescale, genetically targeted optical control of neural activity. *Nat. Neurosci.* **8**, 1263–1268 (2005).
15. Glantz, S. T. et al. Directly light-regulated binding of RGS-LOV photoreceptors to anionic membrane phospholipids. *Proc. Natl Acad. Sci. USA* **115**, E7720–E7727 (2018).
16. He, L. et al. Optical control of membrane tethering and interorganellar communication at nanoscales. *Chem. Sci.* **8**, 5275–5281 (2017).
17. McCubrey, J. A. et al. Roles of the Raf/MEK/ERK pathway in cell growth, malignant transformation and drug resistance. *Biochim. Biophys. Acta* **1773**, 1263–1284 (2007).
18. Chang, F. et al. Signal transduction mediated by the Ras/Raf/MEK/ERK pathway from cytokine receptors to transcription factors: potential targeting for therapeutic intervention. *Leukemia* **17**, 1263–1293 (2003).
19. Vanhaesebroeck, B., Stephens, L. & Hawkins, P. PI3K signalling: the path to discovery and understanding. *Nat. Rev. Mol. Cell Biol.* **13**, 195–203 (2012).
20. Yang, J. et al. Targeting PI3K in cancer: mechanisms and advances in clinical trials. *Mol. Cancer* **18**, 26 (2019).

21. Bugaj, L. J. et al. Cancer mutations and targeted drugs can disrupt dynamic signal encoding by the Ras-Erk pathway. *Science* **361**, eaao3048 (2018).
22. Hino, N. et al. ERK-mediated mechanochemical waves direct collective cell polarization. *Dev. Cell* **53**, 646–660.e8 (2020).
23. Johnson, H. E. et al. The spatiotemporal limits of developmental Erk signaling. *Dev. Cell* **40**, 185–192 (2017).
24. Johnson, H. E. & Toettcher, J. E. Signaling dynamics control cell fate in the early *Drosophila* embryo. *Dev. Cell* **48**, 361–370.e3 (2019).
25. Toettcher, J. E., Gong, D., Lim, W. A. & Weiner, O. D. Light-based feedback for controlling intracellular signaling dynamics. *Nat. Methods* **8**, 837–839 (2011).
26. Toettcher, J. E., Weiner, O. D. & Lim, W. A. Using optogenetics to interrogate the dynamic control of signal transmission by the Ras/Erk module. *Cell* **155**, 1422–1434 (2013).
27. Bugaj, L. J. & Lim, W. A. High-throughput multicolor optogenetics in microwell plates. *Nat. Protoc.* **14**, 2205–2228 (2019).
28. Berlew, E. E., Kuznetsov, I. A., Yamada, K., Bugaj, L. J. & Chow, B. Y. Optogenetic Rac1 engineered from membrane lipid-binding RGS-LOV for inducible lamellipodia formation. *Photochem. Photobiol. Sci.* **19**, 353–361 (2020).
29. Berlew, E. E. et al. Single-component optogenetic tools for inducible RhoA GTPase signaling. *Adv. Biol. (Weinh)* **5**, 2100810 (2021).
30. Hannanta-Anan, P., Glantz, S. T. & Chow, B. Y. Optically inducible membrane recruitment and signaling systems. *Curr. Opin. Struct. Biol.* **57**, 84–92 (2019).
31. Suh, B.-C., Inoue, T., Meyer, T. & Hille, B. Rapid chemically induced changes of PtdIns(4,5)P2 gate KCNQ ion channels. *Science* **314**, 1454–1457 (2006).
32. Regot, S., Hughey, J. J., Bajar, B. T., Carrasco, S. & Covert, M. W. High-sensitivity measurements of multiple kinase activities in live single cells. *Cell* **157**, 1724–1734 (2014).
33. Mayr, V., Sturtzel, C., Stadler, M., Grissenberger, S. & Distel, M. Fast dynamic in vivo monitoring of Erk activity at single cell resolution in DREKA zebrafish. *Front. Cell Dev. Biol.* **6**, 111 (2018).
34. Adrian, M., Nijenhuis, W., Hoogstraaten, R. I., Willems, J. & Kapitein, L. C. A phytochrome-derived photoswitch for intracellular transport. *ACS Synth. Biol.* **6**, 1248–1256 (2017).
35. Golic, A. E. et al. BlsA is a low to moderate temperature blue light photoreceptor in the human pathogen *Acinetobacter baumannii*. *Front. Microbiol.* **10**, 1925 (2019).
36. Nakasone, Y., Ono, T.-A., Ishii, A., Masuda, S. & Terazima, M. Temperature-sensitive reaction of a photosensor protein YcgF: possibility of a role of temperature sensor. *Biochemistry* **49**, 2288–2296 (2010).
37. Nakasone, Y. et al. Stability of dimer and domain–domain interaction of *Arabidopsis* phototropin 1 LOV2. *J. Mol. Biol.* **383**, 904–913 (2008).
38. Richter, F. et al. Engineering of temperature- and light-switchable Cas9 variants. *Nucleic Acids Res.* **44**, 10003–10014 (2016).
39. Benedetti, L. et al. Optimized Vivid-derived magnets photodimerizers for subcellular optogenetics. *eLife* **9**, e63230 (2020).
40. Hernández-Candia, C. N., Casas-Flores, S. & Gutiérrez-Medina, B. Light induces oxidative damage and protein stability in the fungal photoreceptor Vivid. *PLoS ONE* **13**, e0201028 (2018).
41. Van Brederode, M. E., Hoff, W. D., Van Stokkum, I. H., Groot, M. L. & Hellingwerf, K. J. Protein folding thermodynamics applied to the photocycle of the photoactive yellow protein. *Biophys. J.* **71**, 365–380 (1996).
42. Benzinger, D., Ovinnikov, S. & Khammash, M. Synthetic gene networks recapitulate dynamic signal decoding and differential gene expression. *bioRxiv* 2021.01.07.425755 (2021). https://doi.org/10.1101/2021.01.07.425755
43. Duan, L. et al. Understanding CRY2 interactions for optical control of intracellular signaling. *Nat. Commun.* **8**, 547 (2017).

Methods

Cell culture. Lenti-X HEK 293 T cells were maintained in 10% fetal bovine serum (FBS) and 1% penicillin/streptomycin (P/S) in DMEM. NIH 3T3 cells were maintained in 10% calf serum and 1% P/S in DMEM. All cells were cultured in standard cell culture incubators at 37 °C and 5% CO_2. *Drosophila* S2 cells were maintained in Schneider's *Drosophila* medium with 10% heat-inactivated FBS at room temperature. All cell lines were purchased commercially (Lenti-X HEK 293 T cells: Takarabio, catalog number 632180; NIH 3T3: ATCC, catalog number CRL-1658; S2: ThermoFisher Scientific, catalog number R69007). Cell lines were not verified after purchase. Cells were not cultured in proximity to commonly misidentified cell lines.

Plasmid design and assembly. Constructs for stable transduction in mammalian cells were cloned into the pHR lentiviral backbone with an spleen focus forming virus (SFFV) promoter driving the gene of interest. The pHR backbone was linearized using MluI and NotI restriction sites. BcLOV4, iLID, BFP, SOS_{cat} and iSH coding DNA fragments were generated via PCR and inserted into the pHR backbone via HiFi cloning mix (New England Biolabs). For expression in *Drosophila* S2 cells, BcLOV–mCherry, BcLOV–iSH and BcLOV–SOS_{cat} were amplified and inserted into the pbphi-nanos promoter-αTubulin 3′-untranslated region vector[44] between the NheI and BamHI restriction sites. The resulting vectors were digested with NotI and XhoI to replace the nanos protomer with the metallothionein promoter[45], which was synthesized by gBlocks gene fragments (Integrated DNA Technologies). The metallothionein promoter permits inducible expression in the presence of heavy metals, for example, copper. For zebrafish mRNA expression experiments, BcLOV–mCherry, BcLOV–SOS_{cat} and ERK–KTR–BFP (adapted from Regot et al.[32]) were amplified with primers containing att sites for Gateway cloning. PCR amplicons were transferred into pDONR221 plasmids and sequence verified. Gateway cloning was used to transfer each insert into pCSDest plasmids[46].

Plasmid transfection. HEK 293 T cells were transfected using the following calcium phosphate method: per 1 ml of media of the cell culture to be transfected, 50 µl of 2× HEPES-buffered saline (HeBS)[28,29], 1 µg of each DNA construct and H_2O up to 94 µl was mixed. Six microliters of 2.5 mM $CaCl_2$ was added after mixing of the initial components, incubated for 1 min 45 s at room temperature and added directly to the cell culture. S2 cells were transfected with Lipofectamine 3000 reagent (ThermoFisher Scientific) following the manufacturer's protocol. The transfection mixture contained 10 ng µl^{-1} of DNA, 1.5% Lipofectamine 3000 reagent and 2% P3000 reagent, and was brought up to volume with Opti-MEM (ThermoFisher Scientific). The transfection mix was incubated for 15 min at room temperature and was then added directly to the S2 cells. One hundred microliters of transfection mix per 1 ml of cell culture media was used. The transfected cells were imaged 72 h after the transfection (24 h after promoter induction).

Lentiviral packaging and cell line generation. Lentivirus was packaged by cotransfecting the pHR transfer vector, pCMV-dR8.91 (Addgene, catalog number 12263), and pMD2.G (Addgene, catalog number 12259) into Lenti-X HEK 293 T cells. Briefly, cells were seeded one day before transfection at a concentration of 350,000 cells ml^{-1} in a six-well plate. Plasmids were transfected using the calcium phosphate method. Media was removed one day post transfection and replaced with fresh media. Two days post transfection, media containing virus was collected and centrifuged at 800*g* for 3 min. The supernatant was passed through a 0.45-µm filter. Five hundred microliters of filtered virus solution was added to 100,000 NIH 3T3 cells seeded in a six-well plate. Cells were expanded over multiple passages, and successfully transduced cells were enriched through fluorescence-activated cell sorting (BD FACS Aria II) (see gating strategy in Supplementary Fig. 16).

Zebrafish maintenance and mRNA injection. For messenger RNA (mRNA) generation, pCSDest BcLOV–SOS_{cat}, pCSDest BcLOV–mCherry and pCSDest ERK–KTR–BFP were digested with NotI. mRNA was generated using the SP6 mMessage Machine kit (Invitrogen) according to the manufacturer's specifications. 400 pg of BcLOV–SOS_{cat} or BcLOV–mCherry were injected. For the KTR construct, we injected 100 pg. For double injections, mRNAs were mixed before injection. Embryos were derived by natural spawning in the morning of injection and injected with the desired construct(s). Imaging was performed at 24 h post fertilization after embedding the embryos in 1% low melting point agarose in a glass bottom dish. Animal protocols (number 806819) were approved by the University of Pennsylvania Institutional Animal Care and Use Committee (IACUC). Wild-type fish of the AB strain were used for experiments at the indicated time points of development. The sex of the animals cannot be determined at the embryonic stage.

Preparation of cells for plate-based experiments. Plates (with 96 or 384 wells) were seeded with cells, as previously described[27]. Briefly, wells were coated with 50 µl of MilliporeSigma Chemicon Human Plasma Fibronectin Purified Protein fibronectin solution diluted 100 times in PBS and were incubated at 37 °C for 30 min. NIH 3T3 cells were seeded in a 96- or 384-well format at a density of 3,500 or 1,000 cells per well in 100 or 50 µl, respectively and were spun down at 100*g* for 1 min. After 24 h, cells were starved by performing seven 80% washes with starvation media (DMEM + 1% P/S). Experiments were performed after 3 h of starvation.

Optogenetic stimulation. The optoPlate-96 was used for optogenetic stimulation of individual wells in microwell plates[27]. A single-color optoPlate was configured with two blue LEDs for maximum dynamic range of blue-light intensity. The Arduino IDE (v.1.8) was used to program the Arduino Micro found on the optoPlate-96. A low-profile (9 mm tall) well plate adapter was used for experiments in which we simultaneously stimulated and modulated sample temperature. A tall (20 mm) adapter was used for experiments in 384-well plates, as recommended[27]. Stimulation time courses were performed by assigning time points to individual wells. Wells corresponding to different time points were started sequentially, such that all wells could be fixed simultaneously at the end of each experiment. For live-cell imaging experiments, the 488 nm laser was used to stimulate BcLOV4 membrane translocation.

Temperature-controlled optoPlate experiments. Control of sample temperature leveraged the fact that the optoPlate generates heat when operated under conditions that draw large amounts of current[27]. To independently control a sample's illumination conditions and its temperature, we designated 24 LEDs as 'stimulation' LEDs and repurposed the remaining 72 LEDs as 'heater' LEDs (for details see Fig. 2 and Supplementary Fig. 7). Constant illumination of the 72 heater LEDs at varying intensities permitted linear and uniform control of temperature in the 24 sample wells. Experiments were performed with the heatsink fan operating at maximum speed. To perform temperature-controlled experiments, the cell culture incubator temperature was reduced to 25 or 30 °C and optoPlate heating was used to increase temperature according to the relationship described in Fig. 2f. Sample plates were first equilibrated to the lower incubator temperature for 2 h, and then equilibrated on the optoPlate to achieve the desired increased temperature for 1.5 h before the illumination program began.

Immunofluorescence staining. Immediately following completion of a stimulation protocol, 16% paraformaldehyde was added to each well to a final concentration of 4%, and cells were incubated in paraformaldehyde in the dark for 10 min. Cells were then permeabilized with 100 or 50 µl (for 96- or 384-well plates) with PBS + 0.1% Triton X-100 for 10 min. Cells were then further permeabilized with ice-cold methanol for 10 min. After permeabilization, cells were blocked with 1% BSA at room temperature for 30 min. Primary antibody was diluted in PBS + 1% BSA according to the manufacturer's recommendation for immunofluorescence (phospho-p44/42 MAPK (Erk1/2) (Thr202/Tyr204), Cell Signaling, catalog number 4370, 1:400 dilution; phospho-Akt (Ser473), Cell Signaling Technologies, catalog number 9271, 1:800 dilution). Plates (96 or 384 wells) were incubated with 50 or 25 µl of antibody dilution for 2 h at room temperature. Samples were incubated at room temperature in primary antibody for 2 h, after which primary antibody was removed and samples underwent five washes in PBS + 0.1% TWEEN-20 (PBS-T). Cells were then incubated with secondary antibody (Jackson Immunoresearch Alexa Fluor 488 AffiniPure goat anti-rabbit IgG (H+L)) and 4,6-diamidino-2-phenylindole (DAPI; ThermoFisher Scientific, catalog number D1306, 300 nM) in PBS-T + 0.1% BSA for 1 h at room temperature. Secondary antibody was removed, and samples underwent five washes with PBS-T. Samples were imaged in PBS-T.

Imaging. *Live-cell imaging.* Live-cell imaging was performed using a Nikon Ti2E microscope equipped with a Yokagawa CSU-W1 spinning disk, 405/488/561/640 nm laser lines, an sCMOS camera (Photometrics), a motorized stage and an environmental chamber (Okolabs). HEK 293 T cells expressing BcLOV–mCherry were imaged with a ×20 objective at variable temperatures and 5% CO_2. Cells were incubated at the desired temperature for 2 h before imaging to ensure cells equilibrated at the desired temperature. Temperatures were verified by using the temperature sensor shown in Supplementary Fig. 7A. The temperature probes were submerged in PBS in the wells of a 96-well plate, and the probe/plate apparatus was placed on the microscope stage inside the environmental chamber to record temperatures during imaging. BcLOV4 was stimulated using a 488 nm laser. Zebrafish and *Drosophila* S2 cells were imaged at room temperature using a ×40 oil immersion objective.

High-content imaging. Fixed samples were imaged using a Nikon Ti2E epifluorescence microscope equipped with DAPI/FITC/Texas Red/Cy5 filter cubes, a SOLA SEII 365 LED light source and motorized stage. High-content imaging was performed using the Nikon Elements AR software. Image focus was ensured using image-based focusing in the DAPI channel.

Image processing and analysis. *Immunofluorescence quantification.* Images were processed using Cell Profiler[47]. Cells were segmented using the DAPI channel, and cytoplasm was identified using a five-pixel ring around the nucleus. Nuclear and cytoplasmic fluorescence values were then exported and analyzed using R (https://cran.r-project.org/) and R-Studio (https://rstudio.com/). Data was processed and visualized using the dplyr[48] and ggplot2 (ref. [49]) packages. For Fig. 2g,h, exponential decay functions of the form $a \times e^{-b \times x}$ were fit to data points in each condition to visualize the rate of decay in signaling. Curves were fit using the MATLAB R2020a cftool program.

Membrane recruitment. Membrane localization was quantified using the ilastik machine learning software[50]. Briefly, ilastik was used to identify pixels that correspond to the plasma membrane based on user annotations of images of cells that expressed infrared fluorescent protein (iRFP)–CAAX protein, which localizes to the plasma membrane. The resulting image masks were imported into Cell Profiler and were used to quantify the amount of BcLOV4 membrane localization within the same frame. Total BcLOV4, membrane-localized BcLOV4 and total iRFP–CAAX intensity was recorded and further processed in R. Bleaching was corrected by dividing the total intensity of masked mCherry images by the total intensity of mCherry in the original unmasked image. This method assumed that loss of fluorescence was not due to degradation, which we empirically confirmed (Supplementary Fig. 11). Zebrafish and *Drosophila* BcLOV4 membrane recruitment in Fig. 5 was performed by manually comparing the pixel intensity of membrane and cytoplasmic intensities in ten or more cells.

Modeling. The three-parameter model found in Fig. 3 was based on the following observations: (1) The rate of transition from the TI to the dark state can be approximated as 0 because BcLOV4 inactivation is effectively irreversible (Fig. 2c). (2) The rate of BcLOV4 transition from the dark state directly to the TI state can be approximated as 0 because BcLOV4 could be strongly activated even when preincubated for 2 h before stimulation across a wide range of experimental temperatures, with no obvious correlation between temperature and signal strength (Supplementary Fig. 8). (3) The rate of BcLOV4 transition from the TI state to the lit state can be approximated as 0 because temperature-inactivated membrane recruitment and signal activation decay to zero, whereas a nonzero reversion to the lit state would result in a nonzero equilibrium between lit and inactivated state.

Under these assumptions, the following equations were used to model BcLOV4 activity. These equations allow only for bidirectional BcLOV4 movement between the dark and lit states and irreversible movement from the lit state to the TI state.

$$\frac{dD}{dt} = -D \times k_1 + L \times k_2 \quad (1)$$

$$\frac{dL}{dt} = D \times k_1 - L \times k_2 - TI \times k_3 \quad (2)$$

$$\frac{dTI}{dt} = L \times k_3 \quad (3)$$

where D = Dark State BcLOV4, L = Lit State BcLOV4, TI = Temperature Inactivated State BcLOV4, k_1 = Dark to Lit state transition rate, k_2 = Lit to Dark state transition rate, and k_3 = Lit to Temperature Inactivated state transition rate. This system of equations was implemented in MATLAB and was solved numerically using the Euler method. The rate constants k_1, k_2 and k_3 were found by fitting the model to live-cell imaging data of BcLOV4 membrane translocation through minimization of mean squared error (Fig. 3f). Fitting was performed using a custom script that iteratively calculated vertical R-squared across a coarse-grained range of parameter values, and then testing a more finely resolved set of values centered on the best fitting value chosen from the previous iteration. Under the assumption that:

$$k_1, k_2 \gg k_3 \quad (4)$$

k_1 and k_2 were found by setting $k_3 = 0$ and fitting observed BcLOV4 translocation kinetics over short (1 min) periods, yielding the following rate constants:

$$k_1 = 60 \pm 5\,\text{min}^{-1},\ k_2 = 1.5 \pm 0.2\,\text{min}^{-1}$$

k_3 was then determined by keeping k_1 and k_2 constant and fitting k_3 to observed decay rates at each temperature.

The transfer function model of SOS_{cat}-to-ppErk transmission was implemented using the image processing toolbox in MATLAB. Based on previous work[26], we hypothesized that the transfer function could be modeled as a 1° or 2° LPF:

$$1^\circ\ \text{LPF}: \quad H(s) = \frac{\omega_0}{s + \omega_0} \quad (5)$$

$$2^\circ\ \text{LPF}: \quad H(s) = \frac{\omega_0^2}{(s + \omega_0)^2} \quad (6)$$

where $H(s)$ is the ratio between system input and output, s is the complex variable (frequency) and ω_0 is the cutoff frequency. To discriminate between these potential models, we measured ppErk in cells when stimulated by a dynamic 2 min ON/2 min OFF pulse train of light, which corresponds to a frequency that should be ~90% suppressed by the second-order LPF, but substantially less suppressed (~40%) by a first-order LPF (Fig. 4b). We integrated the 1° or 2° LPF models into our model of BcLOV4 translocation, and we fit these integrated models to the data as described above. We found that dynamic Erk stimulation through BcLOV4 translocation was best described by a 1° LPF with a 2-mHz cutoff frequency.

For all experiments related to modeling, illumination duty cycle was used to modulate the intensity of BcLOV4 stimulation. Duty cycle parameters were limited to patterns where the OFF period was less than ~1 min to ensure that BcLOV4 membrane recruitment was maintained at intermediate levels, as determined by its measured inactivation kinetics[15].

Multiplexing experiments. HEK 293 T cells were seeded in a 96-well plate and were cotransfected with 100 ng each of the following plasmids. BcLOV/iLID multiplexing: BcLOV–mCherry, sspb–GFP–P2A–iLID–CAAX and iRFP–CAAX; BcLOV/Cry2 multiplexing: BcLOV–GFP, Cry2(PHR)–mCherry[13]. Images were acquired 24 h post transfection using confocal microscopy. For BcLOV/iLID multiplexing, light stimulation was performed at 37 °C using 1 s of blue light (1.45 W cm^{-2}) every 30 s for 10 min in the presence or absence of prior BcLOV inactivation. Inactivation was achieved using these same light settings for 1 h. For BcLOV/Cry2 multiplexing, 'short light' (10 min) and 'long light' (45 min) exposure was achieved using 100 ms of light (1.45 W cm^{-2}) every 30 s at 30 °C. BcLOV inactivation was achieved using 1 s of blue light (1.45 W cm^{-2}) every 30 s for 45 min. The Cry2-ONLY state was imaged after 45 min of light inactivation.

Reporting Summary. Further information on research design is available in the Nature Research Reporting Summary linked to this article.

Data availability

All raw data used to generate the figures can be found at the following link: https://drive.google.com/drive/folders/1h0eDceDplxYUguSpUNyg5CHA4uudZO39?usp=sharing

Code availability

MATLAB code used to fit data and model BcLOV4 activation dynamics can be found at the following link: https://drive.google.com/drive/folders/1h0eDceDplxYUguSpUNyg5CHA4uudZO39?usp=sharing

References

44. Fukaya, T., Lim, B. & Levine, M. Enhancer control of transcriptional bursting. *Cell* **166**, 358–368 (2016).
45. Santos, M. G., Jorge, S. A. C., Brillet, K. & Pereira, C. A. Improving heterologous protein expression in transfected *Drosophila* S2 cells as assessed by EGFP expression. *Cytotechnology* **54**, 15–24 (2007).
46. Villefranc, J. A., Amigo, J. & Lawson, N. D. Gateway compatible vectors for analysis of gene function in the zebrafish. *Dev. Dyn.* **236**, 3077–3087 (2007).
47. Lamprecht, M. R., Sabatini, D. M. & Carpenter, A. E. CellProfiler™: free, versatile software for automated biological image analysis. *Biotechniques* **42**, 71–75 (2007).
48. Wickham, H., François, R., Henry, L. & Müller, K. dplyr: a grammar of data manipulation. R package v.0.8. 0.1 https://CRAN.R-project.org/package=dplyr (2019).
49. Wickham, H. ggplot2: ggplot2. *Wiley Interdiscip. Rev. Comput. Stat.* **3**, 180–185 (2011).
50. Berg, S. et al. ilastik: interactive machine learning for (bio)image analysis. *Nat. Methods* **16**, 1226–1232 (2019).

Acknowledgements

We thank C. Seiler and the CHOP Aquatic Zebrafish Core for assistance in injecting and mounting zebrafish embryos, D. Wu and D. Chenoweth for assistance with TIRF microscopy and H. Johnson and J. Toettcher (Princeton) for providing *Drosophila* S2 cells. This work was supported by the National Institutes of Health (R35GM138211, R21GM132831 for L.J.B., R35GM133425 for H.D. and B.L., R01NS101106 for E.E.B and B.Y.C. and R01HL152086 to A.F.S.) and the National Science Foundation (Graduate Research Fellowship Program to W.B., CAREER MCB1652003 for E.E.B. and B.Y.C.).

Author contributions

W.B., B.Y.C. and L.J.B. conceived the study. W.B., E.E.B., H.D., I.A.K., A.F.S., C.P. and L.J.B. performed experiments and analyzed data. A.F.S., B.L., B.Y.C. and L.J.B. supervised the work. W.B. and L.J.B. wrote the manuscript and made figures, with editing from all authors.

Competing interests

The authors declare no competing interests.

Additional information

Supplementary information The online version contains supplementary material available at https://doi.org/10.1038/s41589-021-00917-0.

Correspondence and requests for materials should be addressed to Lukasz J. Bugaj.

Peer review information *Nature Chemical Biology* thanks Matias Zurbriggen, Maxwell Wilson and the other, anonymous, reviewer(s) for their contribution to the peer review of this work.

Reprints and permissions information is available at www.nature.com/reprints.

nature portfolio

Corresponding author(s): Lukasz Bugaj

Last updated by author(s): 2021/09/29

Reporting Summary

Nature Portfolio wishes to improve the reproducibility of the work that we publish. This form provides structure for consistency and transparency in reporting. For further information on Nature Portfolio policies, see our Editorial Policies and the Editorial Policy Checklist.

Statistics

For all statistical analyses, confirm that the following items are present in the figure legend, table legend, main text, or Methods section.

n/a	Confirmed	
☐	☒	The exact sample size (*n*) for each experimental group/condition, given as a discrete number and unit of measurement
☐	☒	A statement on whether measurements were taken from distinct samples or whether the same sample was measured repeatedly
☒	☐	The statistical test(s) used AND whether they are one- or two-sided *Only common tests should be described solely by name; describe more complex techniques in the Methods section.*
☒	☐	A description of all covariates tested
☐	☒	A description of any assumptions or corrections, such as tests of normality and adjustment for multiple comparisons
☐	☒	A full description of the statistical parameters including central tendency (e.g. means) or other basic estimates (e.g. regression coefficient) AND variation (e.g. standard deviation) or associated estimates of uncertainty (e.g. confidence intervals)
☒	☐	For null hypothesis testing, the test statistic (e.g. *F*, *t*, *r*) with confidence intervals, effect sizes, degrees of freedom and *P* value noted *Give P values as exact values whenever suitable.*
☒	☐	For Bayesian analysis, information on the choice of priors and Markov chain Monte Carlo settings
☒	☐	For hierarchical and complex designs, identification of the appropriate level for tests and full reporting of outcomes
☒	☐	Estimates of effect sizes (e.g. Cohen's *d*, Pearson's *r*), indicating how they were calculated

Our web collection on statistics for biologists contains articles on many of the points above.

Software and code

Policy information about availability of computer code

Data collection	BD FACSDiva (7.0) Nikon Elements AR (2019) Arduino IDE (v1.8)
Data analysis	Ilastik (1.3) Matlab (R2020a) Matlab cftool (3.5.11) dplyr (1.0.7) ggplot2 (3.3.5)

For manuscripts utilizing custom algorithms or software that are central to the research but not yet described in published literature, software must be made available to editors and reviewers. We strongly encourage code deposition in a community repository (e.g. GitHub). See the Nature Portfolio guidelines for submitting code & software for further information.

Data

Policy information about availability of data

All manuscripts must include a data availability statement. This statement should provide the following information, where applicable:

- Accession codes, unique identifiers, or web links for publicly available datasets
- A description of any restrictions on data availability
- For clinical datasets or third party data, please ensure that the statement adheres to our policy

All raw data and custom code can be found at the following repository: https://drive.google.com/drive/folders/1h0eDceDplxYUguSpUNyg5CHA4uudZO39?usp=sharing

Field-specific reporting

Please select the one below that is the best fit for your research. If you are not sure, read the appropriate sections before making your selection.

☒ Life sciences ☐ Behavioural & social sciences ☐ Ecological, evolutionary & environmental sciences

For a reference copy of the document with all sections, see nature.com/documents/nr-reporting-summary-flat.pdf

Life sciences study design

All studies must disclose on these points even when the disclosure is negative.

Sample size	Sample size in this study correspond to either the number of cells analyed in a condition, or the number of biological replicates performed within one experiment. In fixed cell experiments, cell number was determined by counting the nuclei of cells stained with a fluorescent dye (DAPI). For live cell experiments, sample size was reported as an approximation of the number of cells within the field of view. Cell number in these experiments ranged from 10s-1000s, which allowed high confidence estimation of the mean with small standard error.
Data exclusions	No data points were excluded from analysis
Replication	All experiments were performed either in triplicate and/or were performed independently at least twice , yielding consistent results
Randomization	In these experiments, the same cells were analyzed under all conditions, eliminating the need for randomization
Blinding	Blinding was not performed for most experiments because automated microscopy and quantification eliminated bias. For analysis of ErkKTR experiments in zebrafish, Erk activity was only analyzed in optoSOS expressing fish and thus blinding was not necessary.

Reporting for specific materials, systems and methods

We require information from authors about some types of materials, experimental systems and methods used in many studies. Here, indicate whether each material, system or method listed is relevant to your study. If you are not sure if a list item applies to your research, read the appropriate section before selecting a response.

Materials & experimental systems

n/a	Involved in the study
☐	☒ Antibodies
☐	☒ Eukaryotic cell lines
☒	☐ Palaeontology and archaeology
☐	☒ Animals and other organisms
☒	☐ Human research participants
☒	☐ Clinical data
☒	☐ Dual use research of concern

Methods

n/a	Involved in the study
☒	☐ ChIP-seq
☐	☒ Flow cytometry
☒	☐ MRI-based neuroimaging

Antibodies

Antibodies used	phospho-Erk: Phospho-p44/42 MAPK (Erk1/2) (Thr202/Tyr204) (D13.14.4E). #4370. LOT 4. 1:800 dilution phospho Akt: Phospho-Akt (Ser473) (Polyclonal). Antibody #9271. LOT 4. 1:400 dilution secondary antibody: Goat anti-Rabbit IgG (H+L) Cross-Adsorbed Secondary Antibody, Alexa Fluor 488, A-11008. 1:200 dilution. Polyclonal. LOT: 3.
Validation	Antibodies listed were used in NIH3T3 mouse fibroblasts and S2 Drosophila cells. Validation and references to studies using these antibodies can be found on the manufacturer website.

https://www.cellsignal.com/products/primary-antibodies/phospho-p44-42-mapk-erk1-2-thr202-tyr204-d13-14-4e-xp-rabbit-mab/4370
https://www.cellsignal.com/products/primary-antibodies/phospho-akt-ser473-antibody/9271
https://www.thermofisher.com/antibody/product/Goat-anti-Rabbit-IgG-H-L-Cross-Adsorbed-Secondary-Antibody-Polyclonal/A-11008

Eukaryotic cell lines

Policy information about cell lines

Cell line source(s)	HEK293T: Takarabio NIH3T3: ATCC S2: Thermo Fisher
Authentication	Cells were not authenticated after purchase
Mycoplasma contamination	Cells were tested for mycoplasma twice over the course of this study (PCR and luciferase test), both of which were negative
Commonly misidentified lines (See ICLAC register)	None

Animals and other organisms

Policy information about studies involving animals; ARRIVE guidelines recommended for reporting animal research

Laboratory animals	Wildtype Danio rerio of the AB strain were used for experiments at the indicated time points of development. The sex of the animals cannot be determined at the embryonic stage
Wild animals	None
Field-collected samples	None
Ethics oversight	All animal protocols were approved by the University of Pennsylvania Institutional Animal Care and Use Committee (IUCUC).

Note that full information on the approval of the study protocol must also be provided in the manuscript.

Flow Cytometry

Plots

Confirm that:

☒ The axis labels state the marker and fluorochrome used (e.g. CD4-FITC).

☒ The axis scales are clearly visible. Include numbers along axes only for bottom left plot of group (a 'group' is an analysis of identical markers).

☒ All plots are contour plots with outliers or pseudocolor plots.

☒ A numerical value for number of cells or percentage (with statistics) is provided.

Methodology

Sample preparation	Singe cell suspensions were generated through trypsinization
Instrument	BD FACS Aria II SORP
Software	Cells were sorted using the BD FACSDiva software
Cell population abundance	BFP-positive cells (~1% of the population) were sorted based on gates set on untransduced cells
Gating strategy	Lower bounds of fluorescence were determined by analyzing wild type cells and creating a lower bound that excluded >99.9% of wild type cells.

☒ Tick this box to confirm that a figure exemplifying the gating strategy is provided in the Supplementary Information.